Missing log data interpolation and semiautomatic seismic well ties using data matching techniques

Sean Bader[1], Xinming Wu[1], and Sergey Fomel[1]

Abstract

Relating well-log data, measured in depth, to seismic data, measured in time, typically requires estimating well-log impedance and a time-to-depth relationship using available sonic and density logs. When sonic and density logs are not available, it is challenging to incorporate wells into integrated reservoir studies because the wells cannot be tied to seismic. We have developed a workflow to estimate missing well-log information, automatically tie wells to seismic data, and generate a global well-log property volume using data matching techniques. We first used the local similarity scan to align all logs to constant geologic time and interpolate missing well-log information. Local similarity is then used to tie available wells with seismic data. Finally, log data from each well are interpolated along local seismic structures to generate global log property volumes. We use blind well tests to verify the accuracy of well-log interpolation and seismic well ties. Applying our workflow to a 3D seismic data set with 26 wells achieves consistent and verifiably accurate results.

Introduction

Geophysical reservoir characterization involves careful integration of multiple data sets in an attempt to understand the distribution of subsurface rock properties. An important step of integrating multiple data sets is the seismic well ties, in which well logs are used to calibrate the seismic data, which has lower vertical resolution than the well logs. The calibration typically involves estimating a reflectivity series and time-to-depth relationship (TDR) using the available sonic and density logs (White and Simm, 2003). In plays where sonic and density logs are not acquired in every well, estimating missing logs is an essential step for integrating well-log and seismic data sets.

A simple linear interpolation of missing log data between wells enables estimation of a reflectivity series and TDR; however, it does not account for variations in lithology or structure. Several methods have been proposed to estimate missing logs that could be used for a more accurate seismic well tie. Gardner's equation (Gardner et al., 1974) has been shown to provide a reasonable relationship between sonic and density for a large number of brine-saturated rock types. In addition, the Faust method (Faust, 1953) and Smith method (Smith, 2007) provide empirical relationships between resistivity and sonic logs. Saggaf and Nebrija (2003) note a high interdependence of different log types and apply regularized back-propagation neural networks to estimate missing portions of sonic logs. Each method assumes that specific well logs are collected in every well to carry out the estimation.

An alternative approach is to assume that rock properties do not vary significantly in lateral space, which allows using density and sonic logs from a nearby well to estimate a TDR. Because this assumption does not take into consideration structural or stratigraphic variations in lithology, applying a TDR generated at one well to a nearby well may result in a mistie with the seismic data. To account for these variations, the well must be correlated to a common geologic time. Wheeler and Hale (2014) and Wu et al. (2018) use dynamic time warping (DTW) (Berndt and Clifford, 1994; Hale, 2013) to correlate multiple well logs. Shi et al. (2017a) use the local similarity scan (LSIM) (Fomel, 2007a) to optimally sort and flatten multiple well logs. Once the well logs are flattened or aligned in geologic time, which is analogous to a stratigraphic correlation, missing well-log sections can be estimated from the available data by horizontal interpolation. Bader et al. (2018) flatten well logs from depth to relative geologic time domain and interpolate a missing sonic log using several available sonic logs and several empirical relationships assuming fluid variations have a negligible effect on the well logs.

With a complete well-log suite, including those sonic and density logs estimated by interpolation, we are able to further tie the wells to seismic data. The manual

[1]The University of Texas at Austin, Bureau of Economic Geology, John A. and Katherine G. Jackson School of Geosciences, University Station, Box X, Austin, Texas 78713-8924, USA. E-mail: sbader@utexas.edu; xinming.wu@beg.utexas.edu; sergey.fomel@beg.utexas.edu.

Manuscript received by the Editor 9 February 2018; revised manuscript received 13 October 2018; published ahead of production 07 January 2019; published online 11 March 2019. This paper appears in *Interpretation*, Vol. 7, No. 2 (May 2019); p. T347–T361, 20 FIGS., 2 TABLES.
http://dx.doi.org/10.1190/INT-2018-0044.1.

seismic well tie involves matching common reflectors between the modeled synthetic and seismic data by stretching and squeezing the synthetic until a desired correlation between the data sets is achieved (White and Simm, 2003). To reduce interpreter bias and improve consistency between multiple seismic well ties, several automatic methods have been proposed. Muñoz and Hale (2012) use DTW to automatically align real and synthetic seismograms; this approach is extended to automatically and simultaneously tie multiple wells to seismic by estimating a synthetic image to tie with the seismic image ensuring lateral consistency of the well ties (Muñoz and Hale, 2015). Furthermore, Wu and Caumon (2017) show that laterally consistent seismic well ties can be achieved by using DTW to correlate synthetic and seismic data that are "flattened" to relative geologic time. An alternative approach to carry out the seismic well tie is LSIM; Herrera et al. (2014) compare DTW with LSIM, showing that both methods can successfully compute a seismic well tie. Their study shows that using DTW can achieve a higher correlation between synthetic and seismic data compared with LSIM; however, the resulting TDR using DTW shows an undesirable oscillatory behavior due to stretching and squeezing.

Once each well is tied to the seismic data, the high spatial coverage of seismic can be used to understand lateral variations in log properties. Several methods have been proposed to interpolate log data along local seismic structures. Assuming that available log data are properly tied to seismic and conforms to seismic image features, Hale (2010) uses image guided blended neighbor interpolation (Hale, 2009) for seismic guided well-log interpolation. Alternatively, Karimi et al. (2017) show that predictive painting (Fomel, 2010) can be used to interpolate log data along seismic structures to generate accurate starting models for poststack inversion. Fomel (2016) presents a fast interpolation algorithm for interpolating scattered data to a regularly sampled grid. Interpolation along seismic structure using well-log data generates log property volumes that conform to well-log and seismic data sets. Wu (2017) proposes to compute such a structurally conformable model in the flattened space, in which the seismic and well-log data are unfaulted and unfolded.

In this paper, we address limitations brought about by missing well-log data as well as challenges associated with achieving consistent seismic well ties and propose a workflow that integrates the data matching techniques, LSIM and predictive painting, to estimate missing logs, tie synthetic seismograms to seismic, and finally, interpolate all available well-log data along seismic structures. We use cross validation with a blind well test to test the consistency of seismic well ties. We apply our method to tie 26 wells and the 3D Teapot Dome seismic data set.

Teapot Dome data set

We test the proposed workflow by using the Teapot Dome seismic and well-log data set that were made available by the U.S. Department of Energy and RMOTC. Approximately 1300 wells have drilled into the structure targeting nine reservoirs between 300 and 5500 ft measured depth (Harbert, 2012). The well-log data set contains 900 wells, and we select a subset of 26 wells to test our methods. Also available is a 3D seismic data set (188 crosslines, 345 inlines, sampled at 0.002 s) that is acquired over the selected wells. Figure 1 is a time slice through the 3D seismic volume at 0.72 s illustrating the extent of the 3D seismic data and shows the location of each well. From the time slice, we observe the dome structure and several faults that bisect the structure. These structures are obvious in the crossline shown in Figure 2 and will result in different depth tops

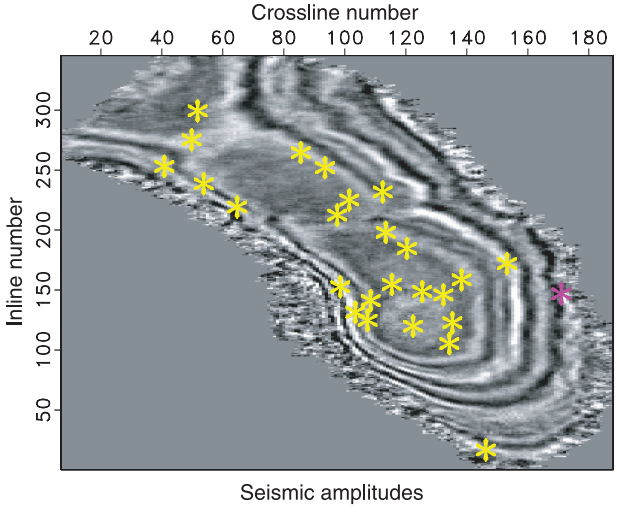

Figure 1. Time slice through seismic data at 0.72 s. The stars indicate the location of each well. The purple well is used as the reference well for missing log data interpolation.

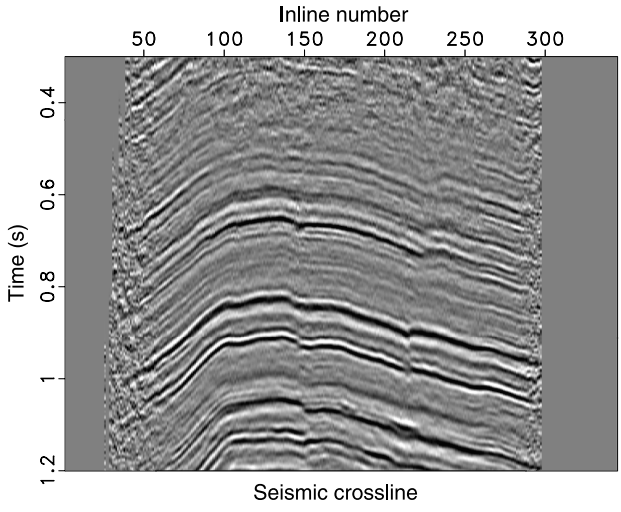

Figure 2. Crossline 126 from available 3D seismic data. The dome structure and several faults that bisect the structure can be observed.

and thicknesses among rock units between wells. An overview of the data set is presented by Harbert (2012).

As discussed later in this paper, not all wells contain sonic and density logs that are required to relate well-log data (in depth) to seismic data (in time), making integration of well-log and seismic data sets challenging. In addition, as the number of wells increases, it becomes more challenging to ensure consistency and accuracy between multiple well ties. Our workflow addresses these limitations and provides a method for validating the results.

Missing log data estimation and seismic well ties

We propose to estimate missing well-log data by first aligning all well logs to a common geologic time. Aligning well logs is analogous to stratigraphic correlation and allows us to interpolate missing sonic and density logs using the available logs. After missing well logs are interpolated, we remove the alignment shifts, thus shifting available and interpolated logs back to the well's original domain. The predicted velocity and density well logs provide the minimum required logs to forward model a synthetic seismogram assuming no changes in fluids between wells. In the next step, synthetic seismograms are modeled using the complete well-log suites at each well location and then are semiautomatically matched with a nearby real seismic trace.

Data alignment using local similarity

Matching data sets involves aligning similar waveforms between two data sets. Whether aligning two logs from different wells or aligning a modeled synthetic seismogram with a seismic trace, we focus on matching a response that corresponds to similar lithologies between the two data sets or a common relative geologic time. In comparing two data sets, our purpose is to estimate the warping function S_k required to align one data set h_k to a reference data set r_k:

$$r_k(t) \approx h_k(S_k(t)). \tag{1}$$

We can represent the warping function $S_k(t)$ as follows:

$$S_k(t) = t + g_k(t), \tag{2}$$

where t denotes the original independent axis and $g_k(t)$ is the shift required to match the data sets as defined in equation 1.

We estimate the warping shifts $g_k(t)$ by using the LSIM method based on the correlation coefficient, which can be used to quantify the quality of the match between data sets (Hampson-Russell, 1999). The LSIM method begins with the observation that the correlation coefficient only provides one number to describe the match; however, we are interested in understanding the local changes in the data sets' similarity. Therefore, the LSIM method computes local similarity c_t, which is a function of time t. The square of c can be split into a product of two factors (Fomel, 2007a):

$$c_t^2 = r_t * h_t, \tag{3}$$

where r_t and h_t are the regularized least-squared inverses (Appendix A). This problem is posed as a regularized inversion where regularization operator is defined using shaping regularization and designed to enforce smoothness (Fomel, 2007b). To visualize LSIM, the inversion is calculated for a series to shifts. The results of this calculation are accumulated and displayed on a "similarity scan" as shown in the following synthetic example. From the similarity scan, we automatically pick

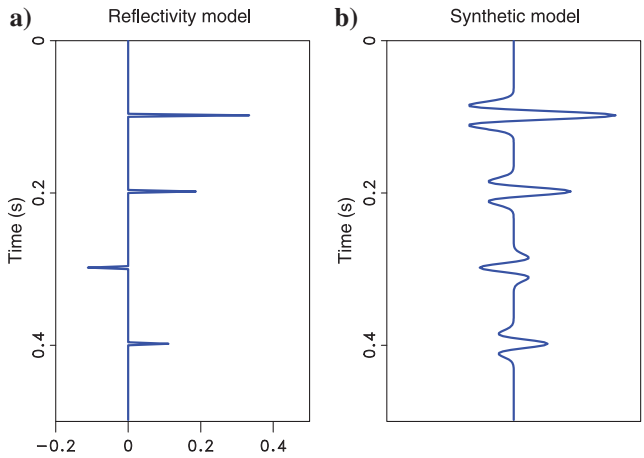

Figure 3. (a) Reflectivity series in time convolved with (b) a 30 Hz Ricker wavelet to model a seismogram.

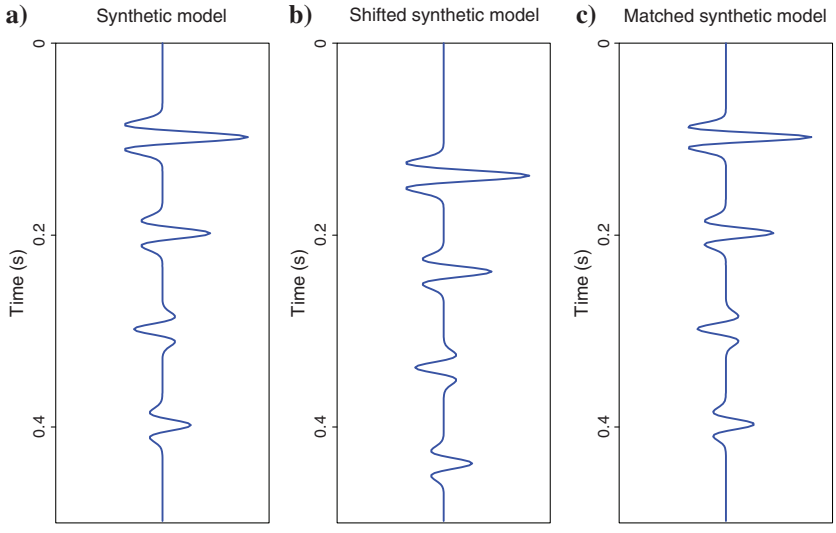

Figure 4. (a) Modeled seismogram, (b) modeled seismogram shifted by 40 ms, and (c) realigned seismogram using the shifts estimated from the LSIM.

the series of shifts along the entire length of the reference data set that optimally aligns the two data sets (Fomel and Jin, 2009).

To illustrate the alignment of two data sets using local similarity, we use two examples based on the simple model shown in Figure 3. In our first example, we apply a 40 ms shift to the modeled synthetic seismogram and use LSIM to estimate the shifts to realign the shifted synthetic model with the original synthetic model (Figure 4). Estimation of the shifts for the first example is visualized in an LSIM shown in Figure 5. In our second example, we add 15% random noise to the reflectivity model and convolve the noisy reflectivity with a 30 Hz Ricker wavelet to create a noisy reference trace. LSIM is used to estimate the shifts to realign the shifted synthetic model with the noisy reference trace in Figure 6. Estimation of the shifts for the second example is visualized in an LSIM shown in Figure 7. From our synthetic examples, we observe that shifts can be accurately estimated to align a modeled seismogram with a noise-free and noisy reference seismograms. We use shifts estimated from local similarity to align multiple well logs and perform seismic well ties.

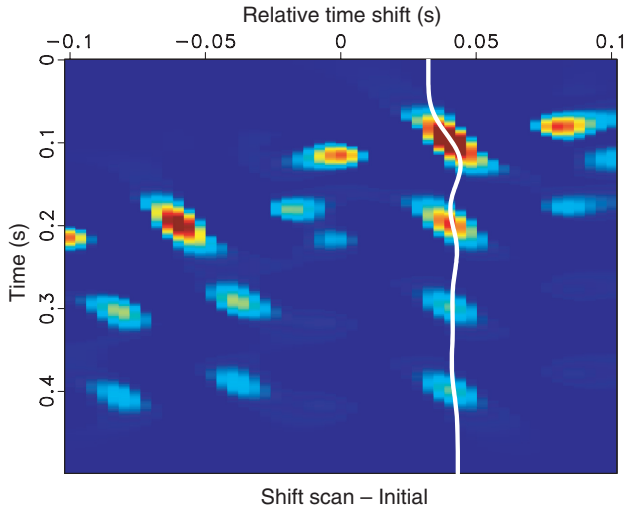

Figure 5. Similarity scan and picked optimal shifts (the white curve). Warm colors represent high similarity, whereas cool colors represent low similarity.

Missing log data estimation

Building on our previous work (Bader et al., 2018), we estimate a complete sonic log using all other sonic logs in the data set and compare it against the actual sonic log from the well. These results are also compared against a conventional approach for estimating missing sonic logs. We then extend the approach to honor true well-log values for well logs that have incomplete or partial well logs.

There are several potential sources of information that can be used to constrain the estimation of missing log data: (1) the same well-log type at other well locations, (2) other well logs within the same well, and (3) the seismic data. We focus on using other well logs of the same type in our estimation of a missing log. In general, we include information from all other wells in our estimation:

$$\begin{bmatrix} \mathbf{W_1} \\ \mathbf{W_2} \\ \vdots \\ \mathbf{W_N} \end{bmatrix} \tilde{l} \approx \begin{bmatrix} \mathbf{W_1}\widehat{\mathbf{l}_1} \\ \mathbf{W_2}\widehat{\mathbf{l}_2} \\ \vdots \\ \mathbf{W_N}\widehat{\mathbf{l}_N} \end{bmatrix}, \tag{4}$$

where our estimated log $\tilde{\mathbf{l}}$ is a weighted function of well logs from different wells denoted by the subscript k. If we simplify the prediction to one unknown log and one known log, equation 4 simplifies to the following linear relationship:

$$W_k(z)\tilde{l}(z) \approx W_k(z)\widehat{l_k}(S_k(z)), \tag{5}$$

where $W_k(z)$ weights the specific value used to estimate the missing log value $\tilde{l}(z)$ from the available well log $\widehat{l_k}(S_k(z))$. To estimate a missing log at each depth sample, we must first remove the structural and stratigraphic variations between the well logs by correlating the well logs to common geologic time using the function $S_k(z)$, based on the shifts estimated from LSIM. The correlation is done by selecting a well-log type that is available in all wells, for example, the gamma ray log. We then select one reference gamma ray log and estimate the function $S_k(z)$ that aligns all remaining gamma ray logs to the reference. The function $S_k(z)$ is applied to the remaining

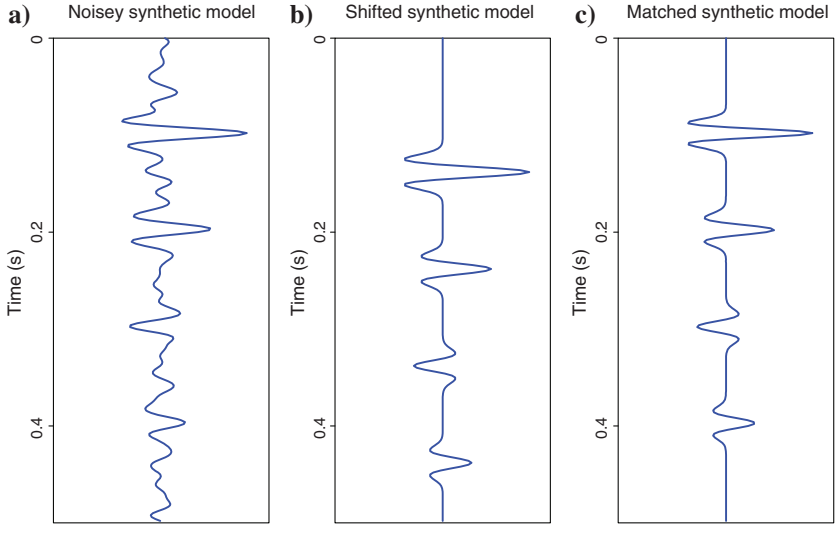

Figure 6. (a) Noisy reference trace, (b) modeled seismogram shifted by 40 ms, and (c) realigned seismogram using the shifts estimated from the LSIM (right).

well logs to align all well logs (density and velocity) to constant geologic time.

We design the weight $W_k(z)$, in equation 5, as a product of two factors: the distance between the unknown and available well logs and the caliper value at that depth, which measures the size of the borehole at each depth. We assume that the borehole is drilled to be a specific diameter and deviations, measured by the caliper, from this anticipated borehole size likely indicates an inaccurate log measurement. Although many environmental factors may impact the well-log data, for simplicity we weight the log values in our inversion based on caliper information. Thus, $W_k(z)$ can be expressed as

$$W_k(z) = \phi(|x - x_k|) * C_k(S_k(z)), \tag{6}$$

where $\phi(|x - x_k|)$ is a radial basis function, x_k is the well location, x is the well with a missing log, and C_k is inversely proportional to the deviation between the expected and actual caliper value at each depth.

There are several different radial basis functions (Powell, 1985). We chose to implement the inverse multiquadratic radial function

$$\phi(|x - x_k|) = \frac{1}{\sqrt{1 + (\epsilon|x - x_k|)^2}}, \quad \text{where } \epsilon > 0 \tag{7}$$

which gives a larger weight to a well closer to the unknown well as compared with a well farther away.

Returning to our original linear relationship, equation 4, the estimated log $\tilde{l}$ is a function of available well logs weighted by each well's distance and caliper log. By solving the least-squares problem in equation 4, we can predict a new "pseudo well log" at each depth as follows:

$$\widetilde{l(z)} = \frac{\sum_{k=1}^{N} W_k^2(z)\widehat{l_k}(S_k(z))}{\sum_{k=1}^{N} W_k^2(z)}. \tag{8}$$

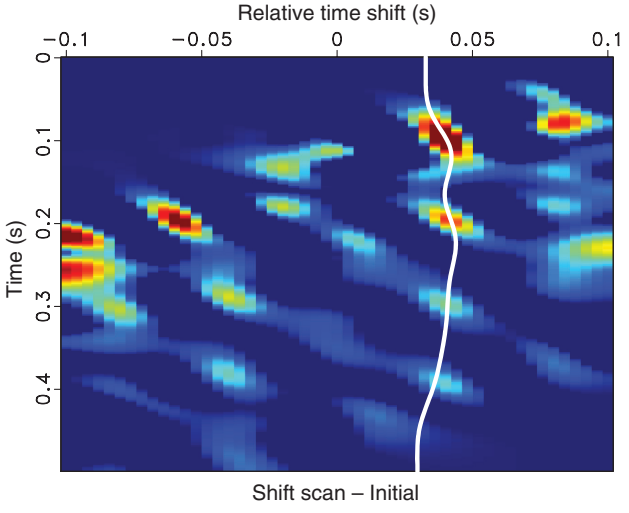

Figure 7. Similarity scan and picked optimal shifts (the white curve). Warm colors represent high similarity, whereas cool colors represent low similarity.

Teapot Dome well-log example

We use wells from the Teapot Dome data set to test the proposed approach. As discussed previously, more than 1000 wells have been drilled into the anticline structure. We select only a limited subset of 26 deepest wells for our examples. Several wells are missing sonic or density logs making it challenging to integrate the available log and seismic data. Table 1 summarizes the parameters of the initial well-log data set.

From equation 1, to align all wells to constant geologic time, we estimate the warping function $S_k(z)$. Because gamma ray logs are available in all wells, we use them to estimate the warping function. The deepest gamma ray log is selected as the reference log $r(z)$, and the well containing this log is denoted by the purple star in Figure 1. The gamma ray and sonic log in the reference well are compared with the gamma ray and sonic log in a different well in Figure 8a and 8b, respectively. The shifts are estimated by matching the gamma ray log from each well to the reference gamma log as shown in Figure 9a. The alignment shifts are then applied to the remaining well logs in each well to align all well logs to constant geologic time. Results of aligning a sonic log before and after applying the shifts estimated from aligning the gamma ray logs are shown in Figures 8b and 9b, respectively.

This approach results in well logs that are flattened along a common geologic time. The log data were collected over several years, with different logging tools, and likely different techniques applied to process the data. To account for this variability, we normalize the sonic and density logs using the big histogram method (Shier and others, 2004). For normalization, we select 15 intervals based on available well-log tops and lithology variations. We estimate the cumulative mean and standard deviation for all well-log data in each interval. We assume that distribution of well-log data from each well, in each interval, should fall within one standard deviation of the cumulative mean. With the aligned and normalized sonic logs, we estimate the missing sonic logs, or sections of sonic logs using equation 8.

We perform a blind well test to validate the proposed approach by estimating a sonic log in a well in which a real sonic log is available. For comparison, we use available density information and the reverse Gardner

Table 1. Original well-log data statistics.

Log type	Wells	Sonic	Density	Caliper	Gamma
Number	26	15	22	26	26
Mean length (ft)	4192	2646	3093	4074	4074

equation (Gardner et al., 1974) to estimate the sonic log; this result is cross plotted against the real sonic log for the entire well in Figure 10a. When estimating the reverse Gardner equation, we break the well into 15 intervals based on the well tops and changes in lithology from the gamma ray log and we recompute the equation that best fits the data for each interval. The estimated sonic log using the proposed approach is cross plotted against the real sonic log for the entire well in Figure 10b. We observe significant improvement in the proposed approach over a conventional method for estimating a missing sonic log. Results comparing the sonic log estimated using the proposed approach against the real sonic log along two 1600 ft intervals are shown in Figure 11. Based on the results of our blind well test using field data, the proposed approach provides a reasonable first-order approximation of the unknown well logs and can be implemented to predict missing well-log data.

From Table 1, we observe that most wells have sonic and density logs; however, the difference between the mean length of the sonic/density logs as compared with the gamma log indicates that several of the well logs were not acquired over specific intervals or have a missing section as shown in Figure 9b. For well logs that have a missing section or are partially complete, we include the available log data in equation 8 to honor the available measurements and interpolate the missing log sections. In Figure 12, we interpolate missing log data in which there are holes in the original log and use true well-log measurements when available.

We applied the proposed approach to all 26 wells from our subset of the Teapot Dome data set to generate complete sonic and density logs for each well. Table 2 summarizes the log data set after estimating missing or incomplete logs.

By estimating missing sonic and density logs for each well, we increase the number of logs and the section of the log available to integrate with the available seismic data. Using the interpolated sonic and density logs, it is possible to compute a TDR and reflectivity series to tie any given well to seismic data.

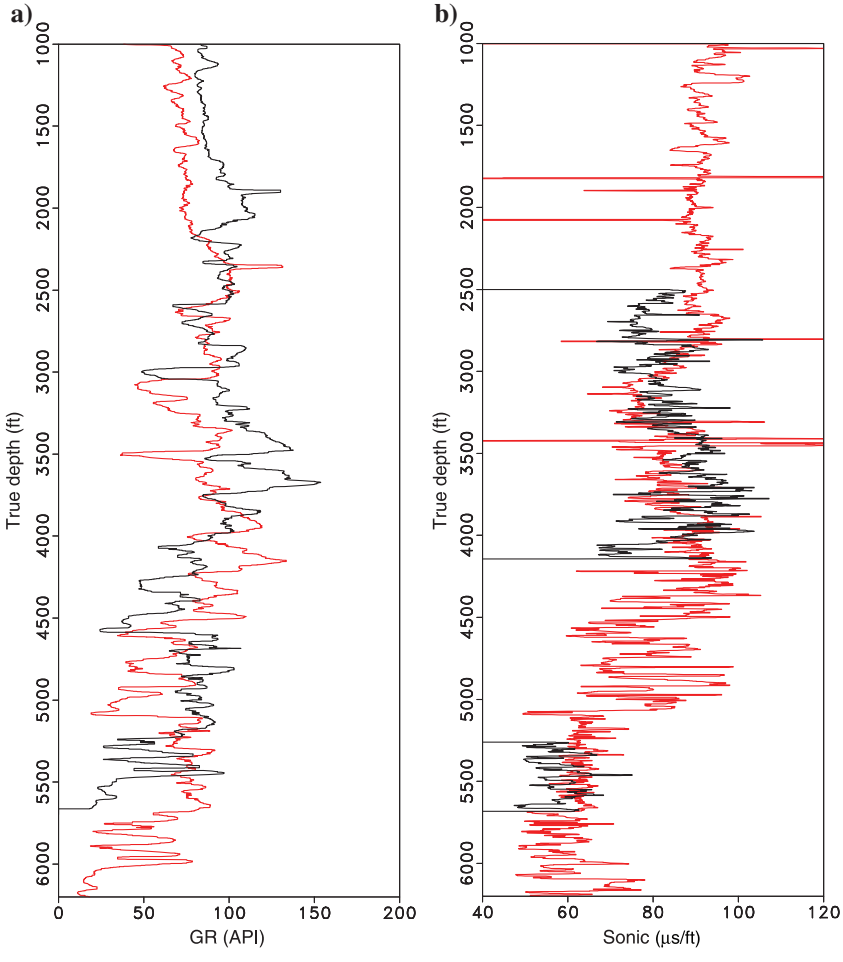

Figure 8. (a) Median filtered gamma log from the reference well (red) and median filtered gamma log from a second well (black) before applying the alignment shifts. (b) Sonic log from the reference well (red) and sonic log from a second well (black) before applying the alignment shifts.

Semiautomatic seismic well ties

Although the log data provide one source of information to understand the subsurface, an additional source of information is the 3D seismic data set. Seismic well ties can be used to calibrate seismic data, which has vertically lower resolution but higher spatial coverage, whereas the well logs can provide vertically higher resolution but are measured only at limited locations.

Synthetic seismograms are modeled independently for each well. White and Simm (2003) argue that modeling synthetic seismograms benefits from blocking or upscaling of the logs. Following their suggestion, we upscale the sonic and density logs to seismic frequencies (Backus, 1962; Marion et al., 1994) and estimate an initial reflectivity series $r_0(z)$ in depth assuming no multiples, attenuation, or dispersion:

$$r_0(z) = \frac{v_0(z+\Delta z)\rho(z+\Delta z) - v_0(z)\rho(z)}{v_0(z+\Delta z)\rho(z+\Delta z) + v_0(z)\rho(z)}, \tag{9}$$

where v_0 is the initial, upscaled, P-wave velocity from sonic in m/s, ρ is the density in gm/cm^3, and Δz is the sampling interval of the log in depth. To relate reflectivity in depth to seismic data in time, we must compute a TDR. There are several ways to compute a TDR. Using available checkshot surveys or vertical seismic profiles can provide accurate measurements of seismic travel-

times to known depths; however, these surveys are not available to us, so we must estimate a TDR from well sonic logs. We define the initial TDR as a function of depth at each well,

$$T_0(z) = 2\int_{z_{\min}}^{z} \frac{d\xi}{v_0(\xi)}, \qquad (10)$$

where T_0 is the initial TDR, $z_{\min}$ is the minimum depth at which sonic information is available, $v_0(z)$ is the initial, upscaled, P-wave velocity from sonic, and $d\xi$ is the depth increment.

The initial TDR relates the initial reflectivity series $r_0(z)$ to time. We interpolate the resulting reflectivity series in time to a regularly sampled grid of 0.002 s, which corresponds to the vertical sampling of the seismic data:

$$r_0(t) = r_0(T_0(z)). \qquad (11)$$

We model synthetic seismograms by convolving $r_0(t)$ with a single, zero-phase, wavelet that is representative of the seismic data's frequency content. The zero-phase wavelet extracted using Hampson-Russell software is shown in Figure 13.

Using the statistical wavelet in Figure 13 and the initial TDR, we compute a synthetic seismogram shown in Figure 14 (green). We then iteratively estimate the alignment shifts g_k by using the LSIM method to match the synthetic seismogram (red) to the corresponding real seismic trace in Figure 14 (black).

In the time domain, the shifts $g_{k,i}(t)$ at well k are estimated using several iterations i of LSIM data matching. Each iteration estimates a smooth sequence of shifts to align the synthetic seismogram with the seismic trace. Muñoz and Hale (2015) and Herrera et al. (2014) observe a relationship between the shifts used to align a synthetic with seismic trace and an updated velocity function.

From equation 2, assuming an initial TDR, T_0, we arrive at updated estimate

$$S_{k,1}(T_0) = T_0 + g_{k,1}(T_0) \qquad (12)$$

after one iteration of LSIM. We estimate an updated TDR by interpolating our shifts from time to depth

$$T_1(z) = T_0(z) + g_{k,1}(T_0(z)). \qquad (13)$$

Using equation 10, we relate the initial and updated velocity log to the initial and updated TDR,

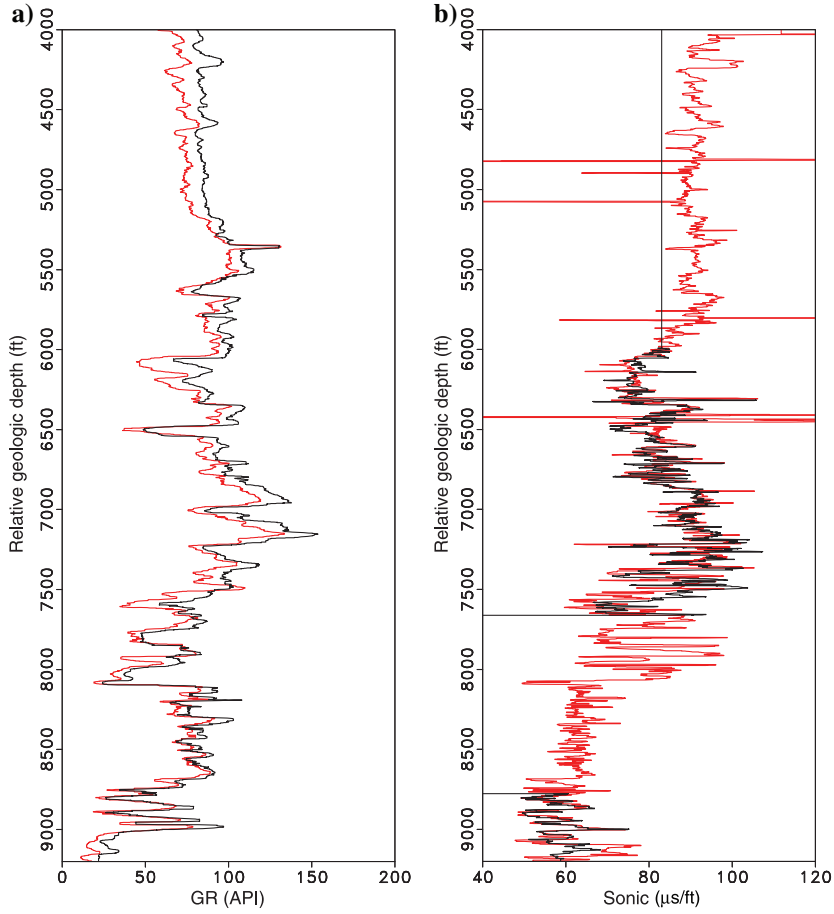

Figure 9. (a) Median filtered gamma log from the reference well (red) and an aligned gamma log from a second well (black) after applying the estimated alignment shifts. (b) Sonic log from the reference well (red) and an aligned sonic log from a second well (black) after applying the estimated alignment shifts from matching gamma logs.

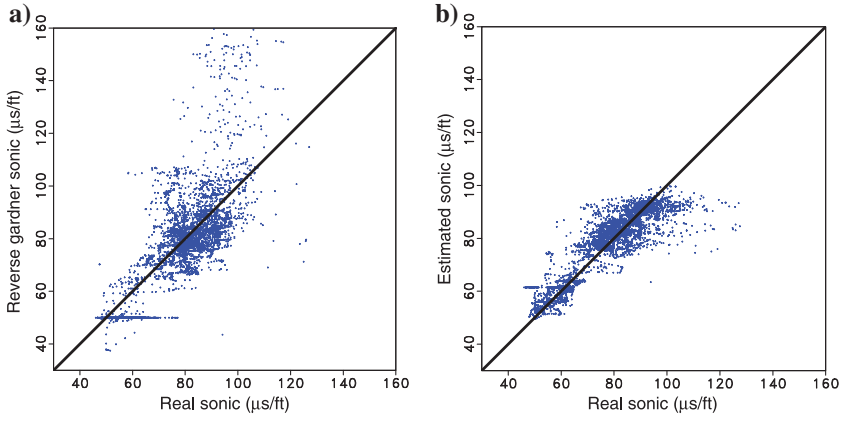

Figure 10. (a) Real sonic log crossplotted against the sonic log estimated using the reverse Gardner equation. (b) Real sonic log crossplotted against the sonic log estimated using the proposed approach.

$$\frac{dT_1(z)}{dz}\left(\frac{dT_0(z)}{dz}\right)^{-1} = \frac{v_0(z)}{v_1(z)} \tag{14}$$

to solve for the updated velocity log,

$$v_1(z) = v_0(z)\frac{dT_0(z)}{dz}\left(\frac{dT_1(z)}{dz}\right)^{-1}. \tag{15}$$

In our implementation, we use equation 15 to update the velocity function after each iteration. Alternatively, we can directly relate the updated velocity log to the initial velocity log and the estimated shifts. Starting with the derivative of equation 13,

$$\frac{dT_1(z)}{dz} = \left(1 + \frac{g_{k,1}(T_0(z))}{dT_0}\right)\frac{dT_0(z)}{dz}, \tag{16}$$

we substitute equation 15 and solve for the update velocity log as follows:

$$v_1(z) = v_0(z)\left(\frac{dg_{k,1}(T_0(z))}{dT_0} + 1\right)^{-1}. \tag{17}$$

We update the velocity function and recompute equations 9–11 after each iteration of estimating shifts using LSIM. We slowly reduce the smoothness enforced by regularization in LSIM with each iteration to ensure that stretching and squeezing are not excessive thus resulting in an improbable velocity update (White and Simm, 2003).

Prior to performing the seismic well tie, we need to understand phase variations and distortions introduced during the processing and imaging of the seismic data. There are several seismic processing and imaging techniques that adjust or correct the seismic data to zero phase. Information on phase adjustments applied to the data is not available; however, Harbert (2012) interprets the deepest continuous reflection to be Precambrian basement resulting in a positive amplitude (in this paper, we define a positive amplitude as related to a positive reflection coefficient). As provided by the U.S. Department of Energy and RMOTC, the basement reflection is a negative amplitude. To account for the observed lateral and vertical phase variations, we apply local skewness correction (Fomel and van der Baan, 2014) resulting in a zero-phased seismic volume consistent with observations from Harbert (2012).

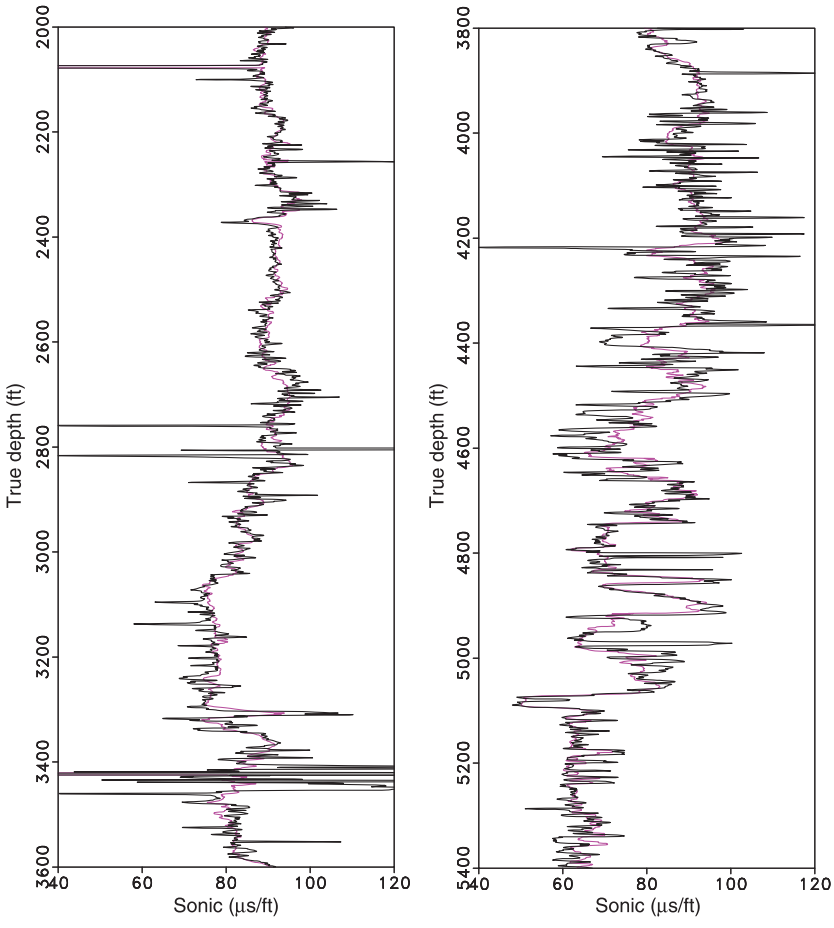

Figure 11. We perform a blind well test by estimating a sonic log using the proposed approach and comparing the result against the real sonic log. The real sonic log (black) versus the estimated sonic log (magenta) along two 1600 ft intervals along the reference log.

Seismic well tie example

To demonstrate our approach, we tie 26 wells using the well-log information summarized in Table 2 and the phase-adjusted 3D seismic data. Each seismic well tie is computed independently by modeling a synthetic seismogram, estimating the shifts using LSIM, and computing an updated velocity function.

One example of a semiautomatic seismic well tie is shown in Figure 14. The synthetic modeled from the original sonic log is compared against the synthetic modeled from a sonic log updated by shifts estimated from four iterations of matching using LSIM and the closest trace from the phase adjusted seismic data set. The high-amplitude reflectors between 0.75 and 1.10 s are well-aligned after four iterations of shifts are estimated to update the sonic log.

The initial Backus-averaged sonic, updated sonic, and original sonic logs are shown in Figure 15a. We observe that most adjustments to the sonic log occur between 3500 and 3900 ft. The adjustment can also be observed by comparing the initial and updated TDRs in

Figure 15b. The differences between synthetic seismograms modeled from well-log data and seismic data are usually attributed to either inaccuracies in the seismic phase or seismic migration velocities (White, 1998; Henry, 2000). The bulk shift between the initial and final TDR is related to the missing shallow velocity section in the well log. The results in Figure 15 provide an initial qualitative assessment of a seismic well tie to ensure that the estimated shifts do not result in an improbable update to the sonic log. We overlay the modeled and tied synthetic seismogram with the crossline that cuts through the well and observe a reasonable tie with the seismic data, even in the presence of a fault (Figure 16).

Validation by interpolation of log data along seismic structures

To qualitatively assess the result of each seismic well tie, we interpolate well-log data from wells along seismic structures. By generating global log property volumes, we can verify the lateral continuity of an log property and perform a blind well test to validate a seismic well tie.

Interpolation using predictive painting

Time dip describes how a seismic event changes from one trace to the next. If available, the local dips could be used to interpolate log data along seismic structure and predict an expected log profile in a location with no well-log data. Similar to Karimi et al.

Table 2. Well-log data statistics after estimating logs for all wells.

Log type	Wells	Sonic	Density	Caliper	Gamma
Number	26	26	26	26	26
Mean length (ft)	4192	3991	3639	4074	4074

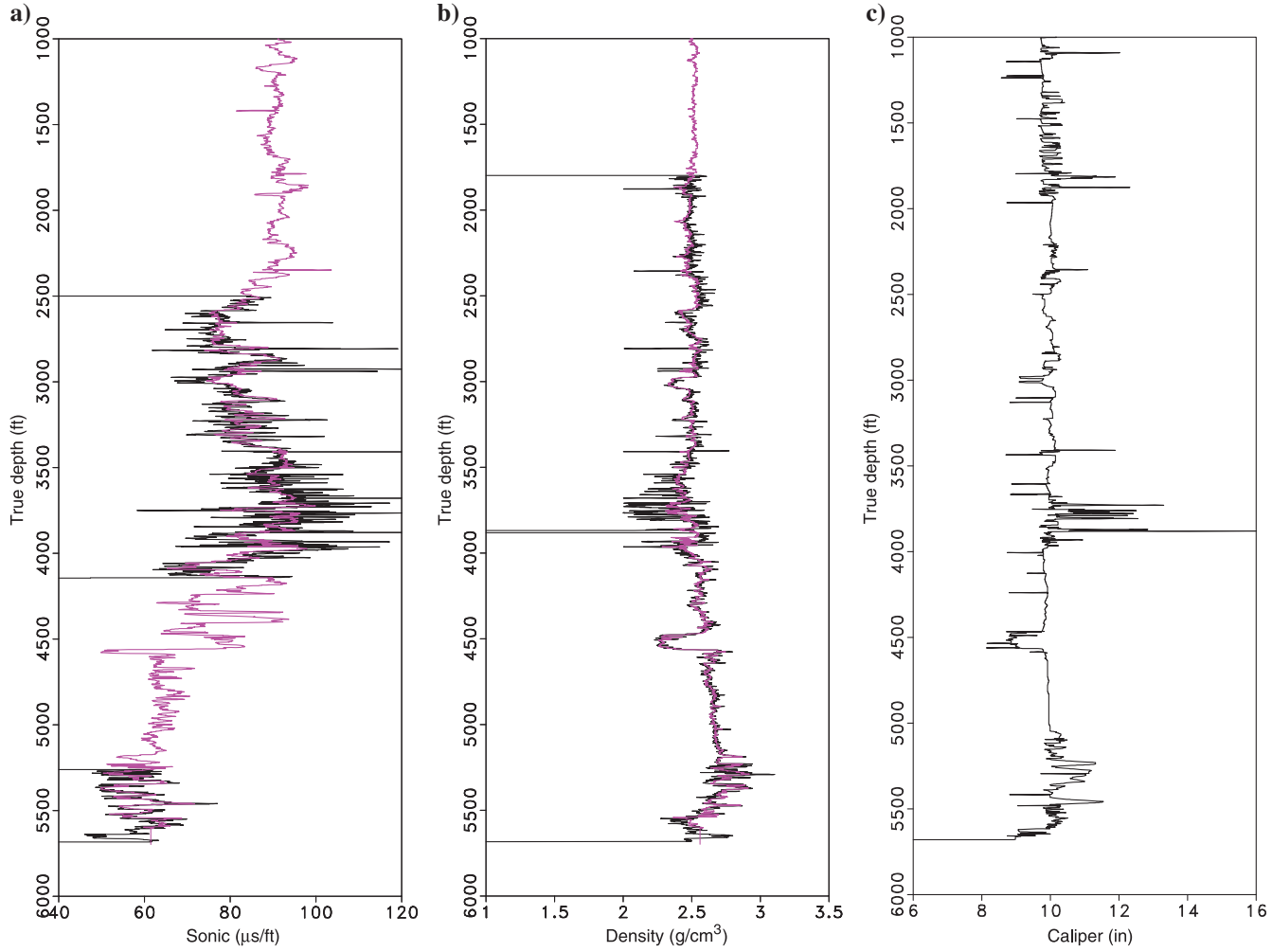

Figure 12. (a) The original sonic log (black) versus the estimated sonic log (magenta). (b) The original density log (black) versus the estimated density log (magenta). The original well-log data are used in the inversion, so in areas where the sonic or density data are available, the estimated logs match the original data. In the interval between 3500 and 3900 ft, there is a significant deviation in the (c) caliper log indicating an inaccurate measurement; therefore, the estimated log deviates significantly from the original log.

(2017), we generate log property volumes by weighting predictive painting. Predictive painting is defined using plane-wave destruction filters that measure the local slope of seismic events (Fomel, 2002). The local slope of seismic events is used to predict one trace from another trace and can be used to interpolate a reference well log through a seismic volume (Appendix B) (Fomel, 2010). The interpolation based on the distance between the reference well and any location is the seismic data set, as defined in equation 7. The RBF and log property volumes generated from data at each well location are combined to form a single log property volume using the following interpolant:

$$V(x,t) = \frac{\sum_k^N \phi(|x - x_k|) S_k(x,t)}{\sum_k^N \phi(|x - x_k|)}, \tag{18}$$

where $\mathbf{S_k}$ is the volume created by spreading log data from location x_k to the entire seismic data set using predictive painting and N is the total number of wells used in the interpolation.

Computing log property volumes

We use 26 wells to compute the log property distribution throughout the Teapot Dome seismic survey. Complete density and sonic logs are estimated and tied to the seismic using the proposed approaches mentioned in the previous sections. Figure 1 is a time slice through the 3D seismic volume at 0.72 s and shows the location of each well. Figure 17a–17c shows the phase adjusted seismic data and estimated inline and crossline dip using plane-wave destruction filters.

The reflection dip is used in the predictive painting algorithm and the RBF interpolant from equation 18 to generate global log property volumes. The inputs to the interpolated sonic volume are the original sonic log interpolated to time using a TDR updated from shifts estimated using four iterations of LSIM matching. The results from interpolating sonic logs from 26 well are shown in Figure 18a. We observe reasonable lateral continuity along seismic structures indicating that there are no significant misties between the well and seismic data. Similar to the interpolated sonic volume, the interpolated the density volume shown in Figure 18b has reasonable lateral continuity along seismic structures and shows no evidence of a mistie. Qualitative interpretation of these results suggests that the estimated well ties are laterally consistent.

Performing a blind well test

The accuracy of the seismic well ties can be additionally checked by removing a well from the interpolation scheme and performing a blind well test. An inconsistent seismic well tie results in a misalignment between the predicted and actual log at the well location. We perform a blind well test using two wells from the 26 well data set. Results shown in Figure 19 indicate a close match between the predicted and actual sonic

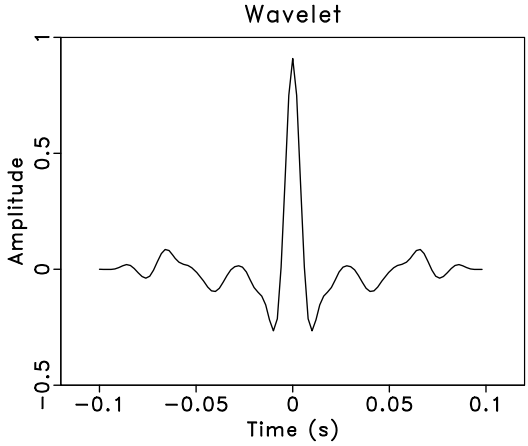

Figure 13. Statistical wavelet extracted from the Teapot Dome seismic data set.

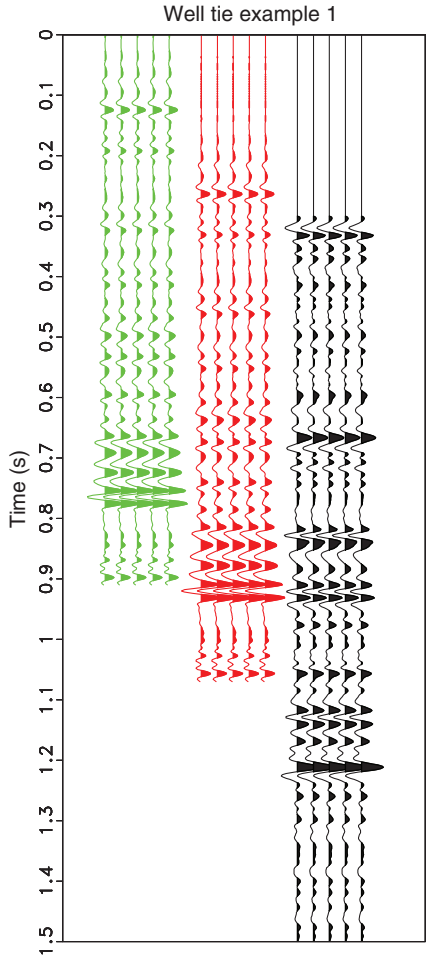

Figure 14. Synthetic modeled using the initial sonic log (green). Synthetic modeled using the sonic log updated after four iterations of matching using LSIM to estimate shifts (red). The closest trace to the well location extracted from the phase adjusted seismic data (black).

log at both well locations confirming the lateral consistency in the seismic well ties.

To understand the accuracy of all seismic well ties, we proceed to perform blind well tests at each well using the remaining wells as input. Results of the actual versus predicted sonic at all 26 wells are cross plotted in Figure 20.

The results shown in Figure 20 indicate the predicted sonic matches reasonably well with the real sonic at all 26 wells giving us confidence that all seismic well ties are consistent and the resulting TDR for each well accurately maps the logs from depth to time.

Discussion

The proposed approach addresses several challenges in integrated studies, specifically (1) interpolating missing well logs at wells that have incomplete well-log suites and (2) providing a methodology for semiautomatically tying wells to seismic and validating the consistency of the ties. In our example, the proposed approach accurately computed a TDR at all well locations regardless of the completeness of the initial well-log suite. Consequentially, integrated studies need not be constrained to pilot wells in which full log suites are collected. The proposed approach should be particularly useful in onshore plays in which the number of wells drilled is much higher compared with the number of sonic and density logs acquired.

Our method involves interpolation techniques that assume that rock properties do not vary significantly laterally. We make several additional assumptions related to the interpolation of missing log data:

1) Gamma logs are matched to estimate the alignment shifts; therefore, estimated section is limited to section in each well with available gamma log.
2) All gamma logs are aligned with a single reference gamma log, and the estimated log section is limited to the stratigraphy found in this reference log. This reference well log can be thought of as a type of log that contains the entire stratigraphic column observed in other well logs.
3) We did not perform fluid substitution prior to solving equation 8 for each well. The proposed approach is based on interpolation, and we assume fluid substitution to have a negligible impact on the results. This assumption may present challenges in reservoirs in which hydrocarbons impact the well-log response within the same stratigraphic interval.

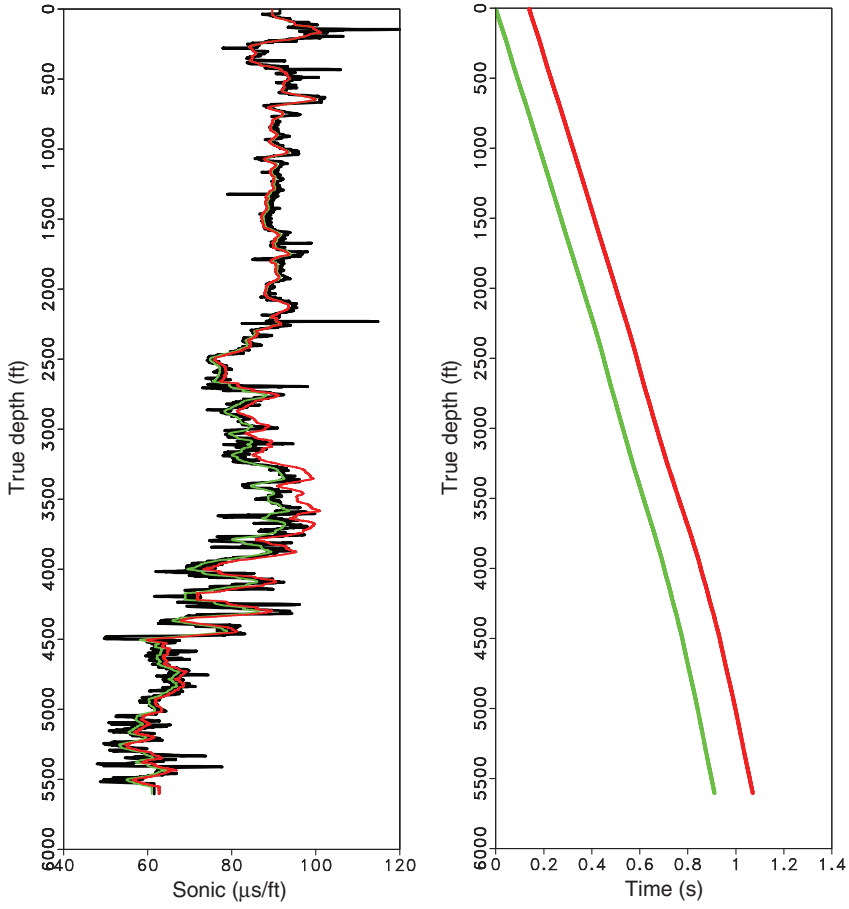

Figure 15. (a) Estimated sonic log using the proposed approach after Backus averaging (green). Updated sonic log after four iterations of matching using LSIM to estimate shifts (red). Estimated sonic log after interpolation of missing data (black). (b) TDR from the estimated sonic log (green). Updated TDR after four iterations of matching using LSIM to estimate shifts (red).

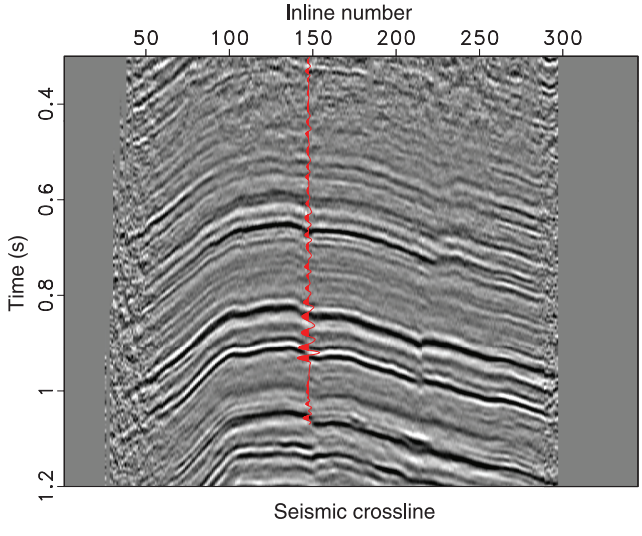

Figure 16. Seismic crossline through the well in Figures 14 and 15. We observe a good tie between the modeled synthetic and real seismic data. The sonic and density logs used to model the synthetic are estimated using the proposed approach.

These assumptions may not be valid in geologically complex areas with significant stratigraphic variations such as unconformities or channels in which entire stratigraphic units may be absent due to erosion. In addition, the well-log correlation approach may meet similar challenges as those experienced by conventional, interpreter-driven workflows in which rapid stratigraphic variability (e.g., slope deposits and clinoforms) may not correlate, or they may correlate ambiguously in several places, between wells. Although we did not account for changes in the fluid content, the proposed approach provides a reasonable first-order approximation of the unknown well logs. The predicted velocity and density well logs provide the minimum required logs to forward model a synthetic seismogram and tie the well with real seismic data.

In addition, well-log data interpolation by predictive painting may result in errors when crossing faults. We observe this challenge when comparing the fault in Figure 17a with the log property volumes in Figure 18. The fault in the property volumes is not accounted for during interpolation. Interpolation schemes that account for discontinuities would further improve results. Recently suggested approaches by Xue et al. (2017) and Shi et al. (2017b) address predictive painting across faults.

Our methodology can also be directly impacted by errors in the seismic data. An incorrect migration velocity will improperly place reflectors, which will result in an incorrect TDR estimated from seismic well ties. Inaccuracies in the migration velocity may be a reason for the need for a velocity log update shown in Figure 15a.

The assumptions we make and errors in migration can compound resulting in inaccuracies in our integrated study. However, by relating several sources of information (multiple well logs and 3D seismic), we provide an approach and validation technique to minimize the impact of these challenges and to provide a better characterization of the subsurface.

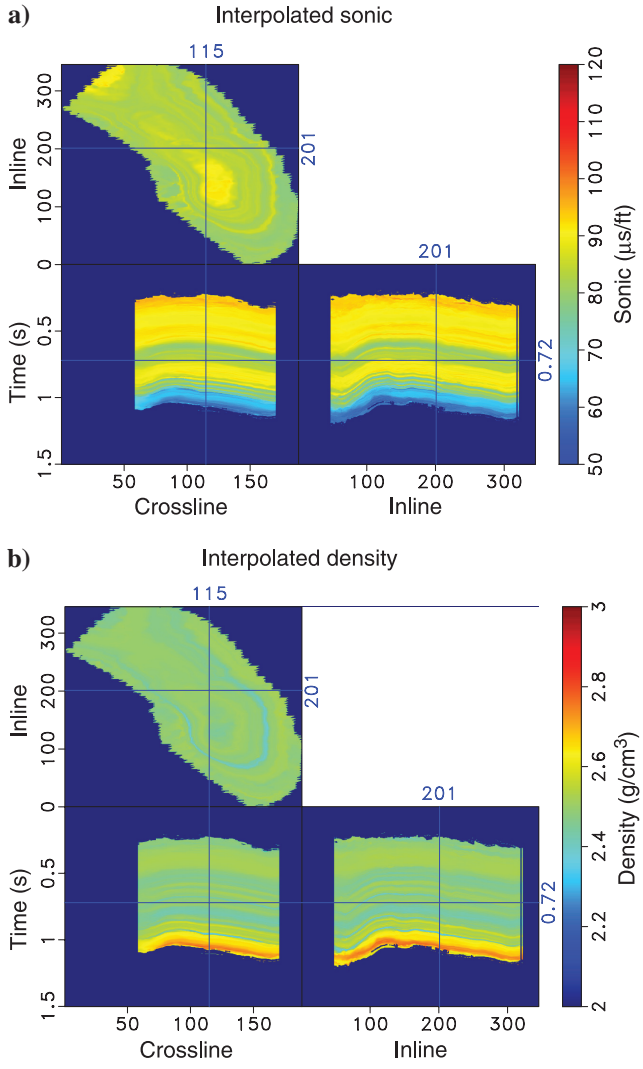

Figure 18. (a) Interpolated sonic and (b) interpolated density based on logs from 26 wells and the interpolant described in equation 18. Note that the interpolated log data follow the seismic structure.

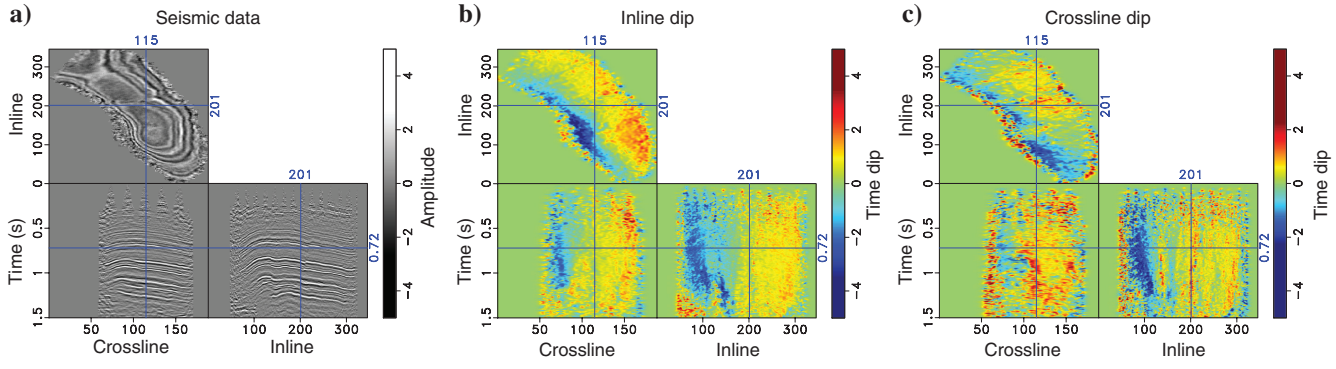

Figure 17. (a) Phase-adjusted seismic amplitude data, (b) inline dip, and (c) crossline dip estimated using plane-wave destruction filters.

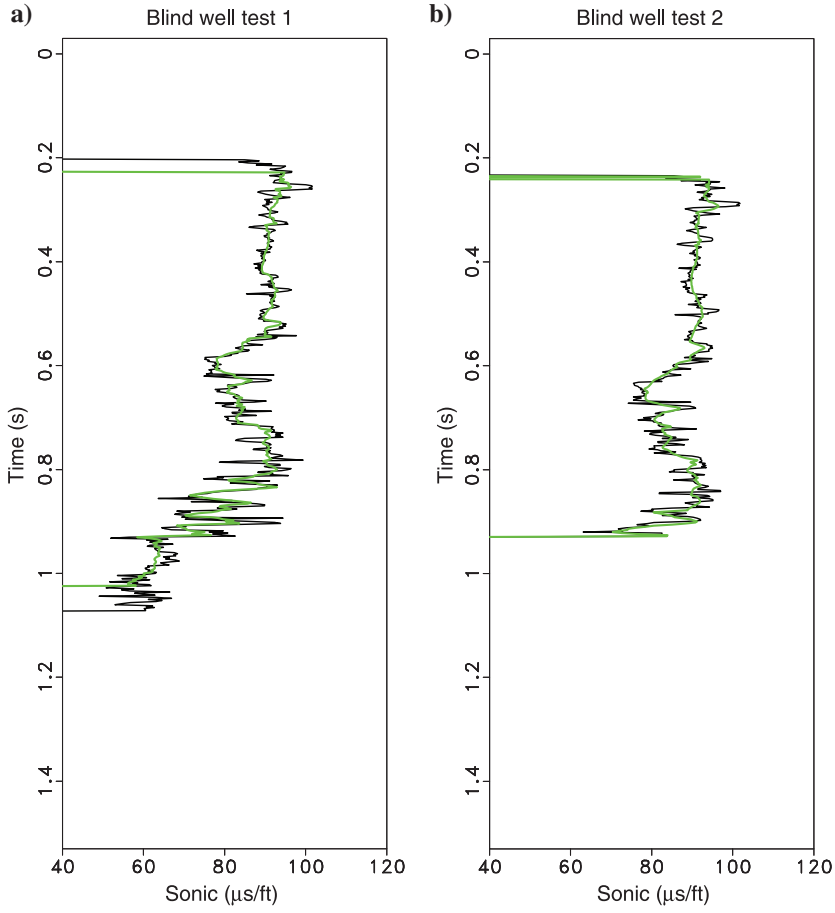

Figure 19. Predicted (green) and actual (black) sonic logs from two different wells using a blind well test. The predicted and actual sonic logs match along the entire length of the well log indicating consistency in seismic well ties.

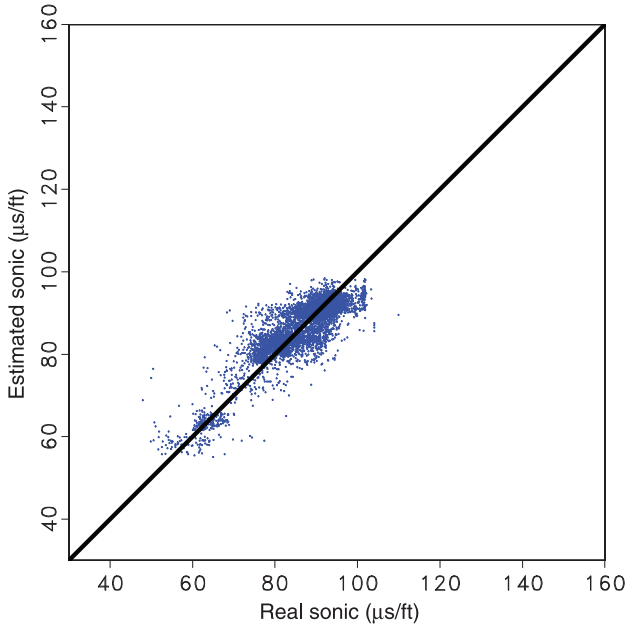

Figure 20. Real sonic log crossplotted against the predicted sonic log from the blind well test for all 26 wells. Each blind well test used the remaining 25 wells as input.

Conclusion

We present a workflow for integrating available well-log data and 3D seismic data. As indicated by computational examples in this paper, the proposed workflow allows us to predict missing or incomplete well-log suites by using LSIM to align all well-log data to common relative geologic time. Therefore, our next step of seismic well ties is not limited to wells that have complete sonic and density well-log data. The wells, with complete or interpolated well-log suites, are tied to a 3D seismic data set using shifts that are semiautomatically estimated using LSIM. The shifts are used to update the initial TDR and sonic logs providing a qualitative assessment of the seismic well tie.

We verify lateral consistency of seismic well ties by interpolating log data from all available wells along seismic structures using predictive painting and performing a blind well test. Our results using well logs and a 3D seismic data set demonstrate that the proposed approach can consistently and accurately tie well-log data to seismic.

The approach has some limitations. In the field data examples reported in this paper, we assume that the reference type log is representative of the entire stratigraphic column found in other wells; this assumption may cause challenges in plays in which rapid stratigraphic variations such as unconformities, channels, or clinoforms may be present. In addition, we did not account for fluid variability in the rocks, which can cause different well-log responses in the same stratigraphic unit. Although fluid substitution may further improve the results, the approach proposed in this paper provides a reasonable, first-order, approximation of the unknown well logs.

Although the uncertainty of the models compared with the true earth model is not considered in this paper, one can assume that each constraint added to the proposed workflow (fluid substitution and modeling) will cast the model into a range of more accurate results. We show, by using field data examples, that the proposed approach is a feasible workflow for overcoming the challenges with the conventional seismic well tie workflows. Further refinement of the well-log information should only improve the results.

The purpose of integrating seismic and well-log data is to achieve reservoir characterization that is most consistent with all available data and achieves the highest possible resolution. Our approach includes previously ignored wells in seismic well ties and provides a method for verifying the consistency and accuracy of the results.

Acknowledgments

We thank the Rocky Mountain Oilfield Testing Center for making the Teapot Dome data set available. We thank the sponsors of the Texas Consortium for Computational Seismology (TCCS) for their financial support. All computations in this paper were done using the Madagascar software package (Fomel et al., 2013).

Data and materials availability

Data associated with this research are available and can be accessed via the following URL: https://wiki.seg.org/wiki/Teapot_dome_3D_survey.

Appendix A

Local similarity

In comparing two data sets, the purpose is to estimate a smoothly varying warping function S_k required to align one data set h_k to a reference data set r_k

$$r_k(t) \approx h_k(S_k(t)). \tag{A-1}$$

We can represent the warping function with the shifts $g_k(t)$ as follows:

$$S_k(t) = t + g_k(t), \tag{A-2}$$

where t denotes the original independent axis and $g_k(t)$ are the shifts required to match the data sets as defined in equation A-1. The correlation coefficient can be used to quantify the quality of the match between data sets (Hampson-Russell, 1999). The LSIM method begins with the observation that the correlation coefficient (c) only provides one number to describe the data sets; however, we are interested in understanding the local changes in the data sets' similarity. Therefore, the LSIM method computes local similarity c_t, which is a function of time t. The square of c can be split into a product of two factors (Fomel, 2007a):

$$c_t^2 = r_t * h_t, \tag{A-3}$$

where r_t and h_t are the solutions to the following regularized least-squares problems, respectively:

$$\min_{r_t}\left(\sum_t (a_t - r_t b_t)^2 + R[r_t]\right)$$
$$\min_{h_t}\left(\sum_t (b_t - h_t a_t)^2 + R[h_t]\right). \tag{A-4}$$

The regularization operator R is implemented using shaping regularization (Fomel, 2007b) and is designed to enforce smoothness. To estimate the solution, LSIM is calculated for a series of shifts. The results of this calculation are accumulated and displayed on a similarity scan.

Appendix B

Predictive painting

We adopt predictive painting to interpolate well-log data along a seismic structure. Predictive painting is defined using plane-wave destruction filters that measure the local slopes of seismic events (Fomel, 2002). The plane-wave destruction operator can be written in linear operator notation:

$$\mathbf{r} = \mathbf{D}\mathbf{s}, \tag{B-1}$$

where $\mathbf{s}$ is a group of seismic traces from a seismic image ($\mathbf{s} = [\mathbf{s}_1\mathbf{s}_2 \dots \mathbf{s}_N]^T$), $\mathbf{r}$ is the destruction residual, and $\mathbf{D}$, the destruction operator, is defined as

$$\mathbf{D} = \begin{bmatrix} \mathbf{I} & 0 & 0 & \dots & 0 \\ -P_{1,2} & \mathbf{I} & 0 & \dots & 0 \\ 0 & -P_{2,3} & \mathbf{I} & \dots & 0 \\ \vdots & \vdots & \vdots & \ddots & \vdots \\ 0 & 0 & \dots & -P_{N-1,N} & \mathbf{I} \end{bmatrix}, \tag{B-2}$$

where $\mathbf{I}$ is the identity operator and $\mathbf{P_{i,j}}$ describes the prediction of trace $\mathbf{j}$ from trace $\mathbf{i}$ by shifting along the local slope of the seismic data. Slopes can be estimated in this way by minimizing the prediction residual operator $\mathbf{r}$ using regularized least-squares optimization. The prediction of one trace from another trace (Fomel, 2010) can be defined as

$$\mathbf{s_k} = \mathbf{P_{r,k}}\mathbf{s_r}, \tag{B-3}$$

where $\mathbf{s_k}$ is the unknown trace and $\mathbf{s_r}$ is the reference trace. The predictive painting operator is defined as

$$\mathbf{P_{1,k}} = \mathbf{P_{k-1,k}} \dots \mathbf{P_{2,3}}\mathbf{P_{1,2}}. \tag{B-4}$$

Predictive painting spreads information along local seismic structures to generate volumes of well-log data from a single well-log reference trace providing a method to predict an expected log profile in a location with no well-log data.

References

Backus, G. E., 1962, Long-wave elastic anisotropy produced by horizontal layering: Journal of Geophysical Research, **67**, 4427–4440, doi: 10.1029/JZ067i011p04427.

Bader, S., X. Wu, and S. Fomel, 2018, Missing well log estimation by multiple well-log correlation: 80th Annual International Conference and Exhibition, EAGE, Extended Abstracts, doi: 10.3997/2214-4609.201800989.

Berndt, D. J., and J. Clifford, 1994, Using dynamic time warping to find patterns in time series: KDD Workshop, 359–370.

Faust, L. Y., 1953, A velocity function including lithologic variation: Geophysics, **18**, 271–288, doi: 10.1190/1.1437869.

Fomel, S., 2002, Applications of plane-wave destruction filters: Geophysics, **67**, 1946–1960, doi: 10.1190/1.1527095.

Fomel, S., 2007a, Local seismic attributes: Geophysics, **72**, no. 3, A29–A33, doi: 10.1190/1.2437573.

Fomel, S., 2007b, Shaping regularization in geophysical-estimation problems: Geophysics, **72**, no. 2, R29–R36, doi: 10.1190/1.2433716.

Fomel, S., 2010, Predictive painting of 3D seismic volumes: Geophysics, **75**, no. 4, A25–A30, doi: 10.1190/1.3453847.

Fomel, S., 2016, Fast scattered data gridding: 86th Annual International Meeting, SEG, Expanded Abstracts, 4059–4063, doi: 10.1190/segam2016-13972078.1.

Fomel, S., and L. Jin, 2009, Time-lapse image registration using the local similarity attribute: Geophysics, **74**, no. 2, A7–A11, doi: 10.1190/1.3054136.

Fomel, S., P. Sava, I. Vlad, Y. Liu, and V. Bashkardin, 2013, Madagascar: Open-source software project for multidimensional data analysis and reproducible computational experiments: Journal of Open Research Software, **1**, e8.

Fomel, S., and M. van der Baan, 2014, Local skewness attribute as a seismic phase detector: Interpretation, **2**, no. 1, SA49–SA56, doi: 10.1190/INT-2013-0080.1.

Gardner, G., L. Gardner, and A. Gregory, 1974, Formation velocity and density — The diagnostic basics for stratigraphic traps: Geophysics, **39**, 770–780, doi: 10.1190/1.1440465.

Hale, D., 2009, Image-guided blended neighbor interpolation of scattered data: 79th Annual International Meeting, SEG, Expanded Abstracts, 1127–1131, doi: 10.1190/1.3255050.

Hale, D., 2010, Image-guided 3D interpolation of borehole data: 80th Annual International Meeting, SEG, Expanded Abstracts, 1266–1270, doi: 10.1190/1.3513074.

Hale, D., 2013, Dynamic warping of seismic images: Geophysics, **78**, no. 2, S105–S115, doi: 10.1190/geo2012-0327.1.

Hampson-Russell, 1999, Theory of the strata program: Technical report, CGGVeritas Hampson–Russell.

Harbert, W., 2012, Rmotc geodatabase: Presented at the SEG IQ Earth Commitee.

Henry, S., 2000, Pitfalls in synthetics: The Leading Edge, **19**, 604–606, doi: 10.1190/1.1438668.

Herrera, R. H., S. Fomel, and M. van der Baan, 2014, Automatic approaches for seismic to well tying: Interpretation, **2**, no. 2, SD9–SD17, doi: 10.1190/INT-2013-0130.1.

Karimi, P., S. Fomel, and R. Zhang, 2017, Creating detailed subsurface models using predictive image-guided well-log interpolation: Interpretation, **5**, no. 3, T279–T285, doi: 10.1190/INT-2016-0051.1.

Marion, D., T. Mukerji, and G. Mavko, 1994, Scale effects on velocity dispersion: From ray to effective medium theories in stratified media: Geophysics, **59**, 1613–1619, doi: 10.1190/1.1443550.

Muñoz, A., and D. Hale, 2012, Automatically tying well logs to seismic data: Center for Wave Phenomena, 253–260.

Muñoz, A., and D. Hale, 2015, Automatic simultaneous multiple well ties: Geophysics, **80**, no. 5, IM45–IM51, doi: 10.1190/geo2014-0449.1.

Powell, M. J., 1985, Radial basis function for multivariable interpolation: A review: Presented at the IMA Conference on Algorithms for the Approximation of Functions and Data, RMCS.

Saggaf, M., and L. Nebrija, 2003, Estimation of missing logs by regularized neural networks: AAPG Bulletin, **87**, 1377–1389, doi: 10.1306/03110301030.

Shi, Y., X. Wu, and S. Fomel, 2017a, Finding an optimal well-log correlation sequence using coherence-weighted graphs: 87th Annual International Meeting, SEG, Expanded Abstracts, 1982–1987, doi: 10.1190/segam2017-17746336.1.

Shi, Y., X. Wu, and S. Fomel, 2017b, Well-log interpolation guided by geologic distance: 87th Annual International Meeting, SEG, Expanded Abstracts, 1939–1944, doi: 10.1190/segam2017-17746077.1.

Shier, D. E. and others, 2004, Well log normalization: Methods and guidelines: Petrophysics, **45**, SPWLA-2004-v45n3a4.

Smith, J. H., 2007, A method for calculating pseudo sonics from e-logs in a clastic geologic setting: Gulf Coast Association of Geological Societies Transactions, **57**, 675–678.

Wheeler, L., and D. Hale, 2014, Simultaneous correlation of multiple well logs: 84th Annual International Meeting, SEG, Expanded Abstracts, 618–622, doi: 10.1190/segam2014-0227.1.

White, R., 1998, Stretch and squeeze — Just keeping up appearances?: 60th Annual International Conference and Exhibition, EAGE, Extended Abstracts, P138, doi: 10.3997/2214-4609.201408412.

White, R., and R. Simm, 2003, Tutorial: Good practice in well ties: First Break, **21**, no. 10, 75–83.

Wu, X., 2017, Building 3D subsurface models conforming to seismic structural and stratigraphic features: Geophysics, **82**, no. 3, IM21–IM30, doi: 10.1190/geo2016-0255.1.

Wu, X., and G. Caumon, 2017, Simultaneous multiple well-seismic ties using flattened synthetic and real seismograms: Geophysics, **82**, no. 1, IM13–IM20, doi: 10.1190/geo2016-0295.1.

Wu, X., Y. Shi, S. Fomel, and F. Li, 2018, Incremental correlation of multiple well logs following geologically optimal neighbors: Interpretation, **6**, no. 3, T713–T722, doi: 10.1190/INT-2018-0020.1.

Xue, Z., X. Wu, and S. Fomel, 2017, Predictive painting across faults: 87th Annual International Meeting, SEG, Expanded Abstracts, 1907–1912, doi: 10.1190/segam2017-17736471.1.

Biographies and photographs of the authors are not available.